Lateral diffusion and aggregation
A Monte Carlo study

Michael J. Saxton

Institute of Theoretical Dynamics, University of California, Davis, California 95616; and Laboratory of Chemical Biodynamics, Lawrence Berkeley Laboratory, University of California, Berkeley, California 94720

ABSTRACT   Aggregation in a lipid bilayer is modeled as cluster–cluster aggregation on a square lattice. In the model, clusters carry out a random walk on the lattice, with a diffusion coefficient inversely proportional to mass. On contact, they adhere with a prescribed probability, rigidly and irreversibly. Monte Carlo calculations show that, as expected, rotational diffusion of the aggregating species is highly sensitive to the initial stages of aggregation. Lateral diffusion of an inert tracer obstructed by the aggregate is a sensitive probe of the later stages of aggregation. Cluster–cluster aggregates are much more effective barriers to lateral diffusion of an inert tracer than the same area fraction of random point obstacles is, but random point obstacles are more effective barriers than the same area fraction of compact obstacles. The effectiveness of aggregates as obstacles is discussed in terms of particle–particle correlation functions and fractal dimensions. Results are applicable to aggregation of membrane proteins, and at least qualitatively to aggregation of gel-phase lipid during lateral phase separation.

INTRODUCTION

The aggregation of proteins in membranes is important in a variety of cellular processes, such as aggregation of receptors for hormones, neurotransmitters, growth factors, and antibodies (Palmer and Thompson, 1989), aggregation of acetylcholine receptors at the neuromuscular junction (Velez et al., 1990), clustering of band 3 by denatured hemoglobin in abnormal or senescent erythrocytes (Schlüter and Drenckhahn, 1986; Waugh et al., 1986), and aggregation of virus glycoproteins in the plasma membrane of an infected cell (Petersen et al., 1986).

An aggregation model may also be useful as a qualitative model of lipid lateral phase separation induced by changes in temperature, lateral pressure, or cation concentration. In a study of gel-phase structures in phospholipid monolayers at the air–water interface, Flörsheimer and Möhwald (1989) propose a two-step process in which submicroscopic domains grow and then aggregate. Sun and Petersheim (1990) suggest a similar picture in their work on cation-induced phase separation.

An understanding of aggregation models is useful to establish the role of aggregation in membrane processes. The cluster–cluster aggregation (CCA) model has been extensively studied (Jullien and Botet, 1987; Meakin, 1988; Vicsek, 1989). In this model, clusters move by a random walk on a lattice, and clusters which come into contact adhere rigidly and irreversibly. The process continues until only one cluster is left. The only interactions included are hard-core repulsion and sticking. The CCA model is distinct from diffusion-limited aggregation, in which there is initially one stationary seed particle. Single particles move by a random walk, and bind irreversibly when they come into contact with the seed particle or a previously bound particle (Meakin, 1988; Vicsek, 1989).

These aggregates can be characterized in several ways. First, we examine the particle–particle correlation function, which yields a correlation length and the fractal dimension of the clusters. Next, we examine the effect of the aggregates as obstacles to diffusion, and find that the aggregates are much more effective barriers than the same area fraction of random point or square obstacles. Finally, we examine the translational and rotational diffusion coefficients of the clusters.

METHODS

The CCA calculations are carried out by standard methods (Meakin, 1983; Kolb et al., 1983). A 256 × 256 square lattice with periodic boundary conditions is used. To begin the calculation, particles are placed on randomly chosen sites, without overlap; particles that are initially adjacent are assumed to form a cluster. Then the clusters execute a random walk. Whenever two clusters become adjacent, an attempt is made to merge the clusters, with a prescribed probability P_{AGG}. If the clusters are merged, they are merged irreversibly into a rigid cluster, and move as a unit thereafter. If the clusters do not merge, they remain adjacent but unconnected, and may separate on a later move. The random walk continues until only one cluster remains. The aggregation time is defined as the time required to form the final cluster.

Further rules on cluster mergers are as follows. If a single point in

one cluster is adjacent to two points in another cluster, or if two points in one cluster are adjacent to two points in another cluster, two attempts are made to merge the clusters. The clusters are merged if one or both attempts are successful. In an unmerged adjacent pair, if one cluster tries a move that would cause the clusters to overlap, the move is blocked, but the appropriate attempts to merge the clusters are made.

Points in clusters are identified using linked lists. Clusters are identified using the algorithm of Hoshen and Kopelman (1976), modified to allow for periodic boundary conditions.

The translational diffusion coefficient of a cluster is assumed to be $D_T(CL) = M_{MIN}/M$, where M is the mass of the cluster, and M_{MIN} is the mass of the smallest cluster present at that time (Meakin et al., 1985). At each step, a cluster is chosen at random, the clock is incremented by an amount Δt defined below, the diffusion coefficient $D_T(CL)$ of the cluster is calculated, and a random number r between 0 and 1 is generated. If $r < D_T(CL)$, the cluster is moved in a random direction; otherwise, the cluster is not moved. The normalization of $D_T(CL)$ implies that the smallest cluster moves every time it is chosen.

Each step in the program corresponds to a physical time increment of $\Delta t = M_{MIN}/N(t)$, where $N(t)$ is the number of clusters present at time t (Meakin et al., 1985). The factor of $1/N(t)$ makes the unit of time one move per cluster, avoiding an artifactual acceleration of time during the calculation. If 100 clusters are present, then 100 steps correspond to one move per cluster, but when only two clusters are present, 100 steps correspond to 50 moves per cluster (Vicsek and Family, 1984). The factor of M_{MIN} is required because the smallest cluster moves every time it is chosen. Consider the step at which the last unit cluster merges with another cluster. Before this step, a cluster of mass 2 moves with probability ½, and $\Delta t = 1/N(t)$. After this step, a cluster of mass 2 moves with probability 1, but $\Delta t = 2/N(t)$.

The aggregation process is stopped at prescribed times, the clusters are characterized, and the aggregation process is continued. Cluster masses and the radius of gyration are averaged over 100 different configurations.

The particle–particle correlation function is obtained by Fourier transformation (Press et al., 1986). The correlation length and the fractal dimension are obtained from a log–log plot of the correlation function versus radius, as described below. The correlation function is averaged over 100 different configurations.

Cluster sizes are described by the radius of gyration $R_{GYR}^2 = (1/M)\Sigma_i(r_i - r_0)^2$, where r_i is the position of the ith particle of the cluster, r_0 is the position of the center of mass, and M is the mass of the cluster. This is calculated assuming that the clusters are made up of point particles.

The rotation diffusion coefficient of a cluster is $D_R(CL) \sim 1/R_H^2$ (Saffman and Delbrück, 1975), where the hydrodynamic radius R_H is assumed to be proportional to the radius of gyration. To avoid a divergence for clusters of unit mass, we assume that the cluster is made up of circles of radius $\ell/2$, where ℓ is the lattice constant, and calculate the radius of gyration by standard means (Synge and Griffith, 1949). The rotational diffusion coefficient is then

$$D_R^*(CL) = 1/[M(1 + 8R_{GYR}^2)], \qquad (1)$$

which is normalized to one for a cluster of unit mass.

Diffusion calculations are carried out as described earlier (Saxton, 1987). The positions of the clusters are fixed, and a tracer is placed at a random unblocked point on the lattice. The tracer then carries out a random walk on lattice sites not occupied by a cluster, and the position of the tracer is recorded periodically. The calculation is repeated for various starting positions of the tracer, and various aggregates at the same concentration and aggregation time. The mean-square displacement of the tracer is obtained as a function of time, and the diffusion coefficient is obtained as described earlier (Saxton, 1987). The

diffusion coefficient is normalized to one when no obstacles are present. For short runs (10^5 time steps), 400 different tracers and 100 different aggregates were used; for long runs (2×10^6 time steps), 100 tracers and 25 aggregates. Calculations for diffusion of a tracer in the presence of random point or square obstacles were carried out similarly. To evaluate the statistical error, several independent runs were made. For final aggregates at an area fraction of 0.1, $D^* = 0.170 \pm 0.013$ (5 runs). For random points at an area fraction of 0.3, $D^* = 0.264 \pm 0.003$ (6 runs). For random points, twice as many tracers and twice as many repetitions were typically used.

RESULTS AND DISCUSSION

The cluster–cluster aggregation model

In the CCA model, point particles are placed at random on a lattice at a prescribed concentration. The clusters then move by a random walk. When two clusters become adjacent, they adhere with a prescribed sticking probability P_{AGG}. If they adhere, they are joined rigidly and irreversibly; if they do not adhere, they may separate on a later move. The process continues until only one cluster remains. Here $P_{AGG} = 1$ corresponds to diffusion control, and $P_{AGG} = 0$, to reaction control (Kolb and Jullien, 1984).

The calculations are carried out on a square lattice, to represent aggregation of a tetravalent species. To simulate lateral phase separation in a lipid, a triangular lattice is more appropriate; this case will be treated in later work. Periodic boundary conditions are imposed.

The translational diffusion coefficient $D_T(CL)$ of a cluster is assumed to be inversely proportional to the mass of the cluster. Although the form of $D_T(CL)$ affects the time dependence of the cluster size distribution, it does not affect the structure of the final cluster significantly, provided that small clusters diffuse faster than large clusters (Meakin, 1984a). Rotational diffusion is not allowed; it has little effect on the fractal dimension of the final cluster (Meakin, 1984b). Clusters from off-lattice and on-lattice simulations have similar fractal dimensions (Meakin, 1985).

The concentration of obstacles, C_0, is expressed as an area fraction, defined as the fraction of lattice points occupied by particles. The unit of length is the lattice constant ℓ. To translate calculated quantities into observable quantities, ℓ may be taken to be the size of a lipid or the size of a protein.

If the lattice spacing is assumed to be an appropriate value for a lipid, $\ell = 0.8$ nm, and the diffusion coefficient of a monomer is assumed to be $D_T = 5$ $\mu m^2/s$, then the jump time is $\langle r^2 \rangle/4D_T = 32$ ns. For $C_0 = 0.1$, $P_{AGG} = 1$, and a 256 × 256 grid, the mean aggregation time is $\sim 8 \times 10^5$, or ~ 25 ms, and the size of the grid is ~ 0.2 μm. For the assumed value of D_T, the rotational diffu-

sion coefficient of a monomer is $D_R = 4.8 \times 10^6$ s^{-1} (Saffman and Delbrück, 1975). (We assume, in their notation, a particle radius $a = \ell/2 = 0.4$ nm, a membrane thickness $h = 5$ nm, and viscosities of 1 poise for the lipid phase and 0.01 poise for the aqueous phase.)

Similarly, for aggregation of proteins the size of the erythrocyte band 3 anion transport protein, we have $\ell = 6.6$ nm (Weinstein et al., 1979) and $D_T = 1.8$ μm^2/s for band 3 in a dimyristoylphosphatidylcholine bilayer at 35° C (Clegg and Vaz, 1985), so that the jump time is 6 μs. The aggregation time of 8×10^5 then corresponds to 4.8 s, and the size of the grid is 1.7 μm. For this value of D_T, the Saffman-Delbrück equation predicts $D_R = 3.7 \times 10^4$ s^{-1}, in good agreement with experiment (Clegg and Vaz, 1985).

Time course of aggregation

Some examples of aggregates are shown in Fig. 1. Fig. 1, a–e shows the time course of aggregation for an area fraction $C_0 = 0.1$ and a sticking probability $P_{AGG} = 1.0$. Initially, the particles are randomly distributed and only small clusters are present. As aggregation proceeds, the clusters are of a roughly uniform size and distribution (Kolb, 1984). Finally, only one cluster is present, with an extended, stringy structure. Fig. 1 f shows a final cluster for $C_0 = 0.05$, $P_{AGG} = 1.0$. Even with such a low concentration of particles, the cluster is extended enough to have a significant effect on lateral diffusion. Figs. 1 g and h show final clusters for $C_0 = 0.20$ and $C_0 = 0.30$, $P_{AGG} = 1.0$.

The stringiness of the final cluster is a result of the assumption that the particles adhere irreversibly and with unit probability on contact. If the particles can detach and reattach, or if the probability of adhesion is small, the cluster forms a more compact structure, with a higher fractal dimension (Kolb and Jullien, 1984; Shih et al., 1987). Contrast Fig. 1 g, a final cluster for $C_0 = 0.2$, $P_{AGG} = 1$ with Fig. 1 i, for $C_0 = 0.2$, $P_{AGG} = 0.001$. When P_{AGG} is small, the clusters are thicker and less stringy, because neighboring clusters can penetrate each other more deeply before adhering.

Cluster growth and structure can be characterized in several ways. Growth can be described by the various average molecular masses used to characterize polymers (Tanford, 1961; Meakin, 1984c). If M_i is the mass of the ith cluster and N is the total number of clusters, then the number-average cluster mass is $M_N = \Sigma_i M_i/N$, and the mass-average cluster mass is $M_M = \Sigma_i M_i^2/\Sigma_i M_i$. The ratio M_M/M_N is a measure of the uniformity of the cluster size. For uniform clusters, the ratio is 1; for a linear condensation polymer of random length, the ratio is 2 (Tanford, 1961). The cluster size is described by the radius of gyration R_{GYR}, defined in Methods. A simple measure of

cluster structure is the average coordination number $\langle Z \rangle$. Values of these quantities are shown in Fig. 2. For $P_{AGG} = 1$, the average masses increase roughly as $t^{0.6}$, the number of clusters varies roughly as $t^{-0.6}$, and the radius of gyration increases as $t^{0.43}$. The ratio M_M/M_N remains approximately constant, reflecting the uniformity of the clusters as shown in Fig. 1. The average coordination number $\langle Z \rangle$ reaches its asymptotic value early in the aggregation process. As shown in Fig. 2 c, the radius of gyration is smaller for $P_{AGG} = 0.01$ than for $P_{AGG} = 1$, reflecting the more compact structure obtained when P_{AGG} is small.

Fractal structure

The cluster structure may be characterized by the particle-particle correlation function $C(r)$, giving the probability that, if a particle is at $r = 0$, there is also a particle in any cluster at a distance r. (One could also define a correlation function giving the probability that if a particle is at $r = 0$, there is also a particle in the same cluster at a distance r [Martin and Wilcoxon, 1989].) This correlation function could be obtained experimentally from electron micrographs.
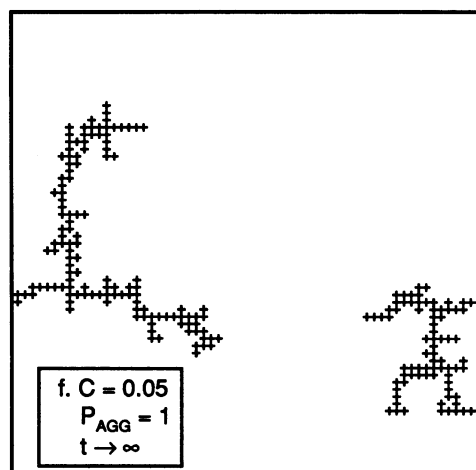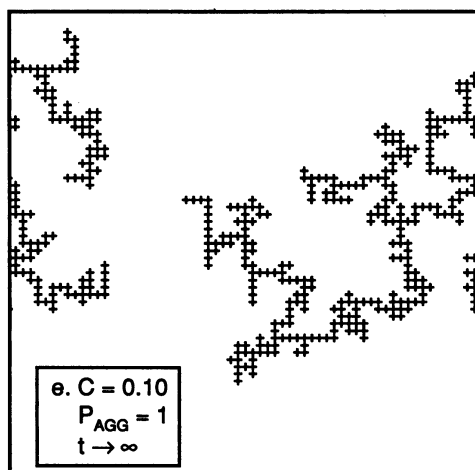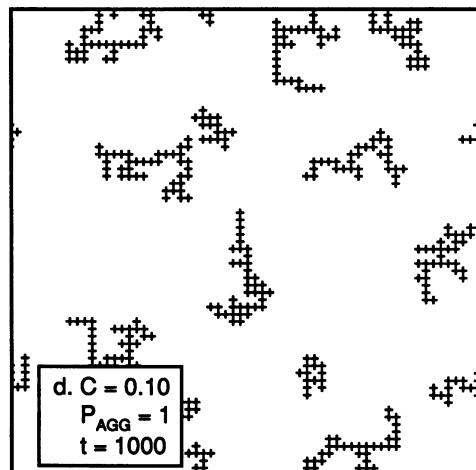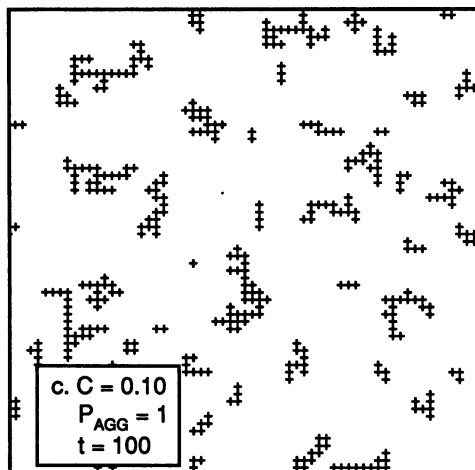
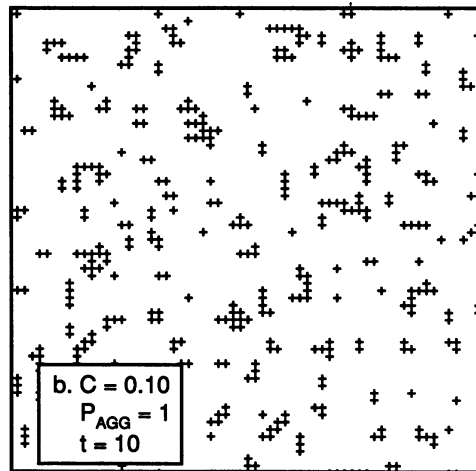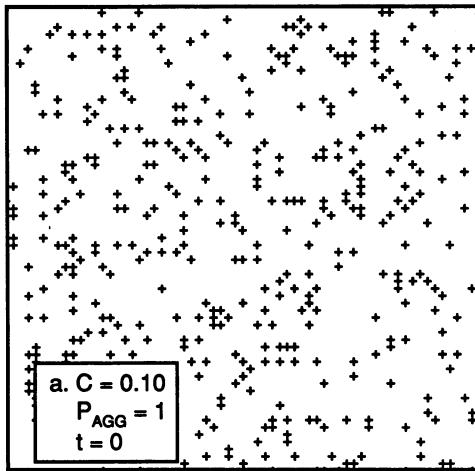Initially, the distribution is random and $C(r)$ is constant for all $r > 0$, as shown in Fig. 3 a. As clusters form, a peak builds up at small r, representing the clusters, and a shallow valley develops at larger r, representing the depletion of particles in the region between the clusters.

The final aggregate has a fractal structure at short length scales, and a uniform structure at large length scales, as shown in the correlation function

$$C(r) \sim \begin{cases} 1 & (r = 0) \\ r^{-(d-D_f)} & (r \ll R_{COR}) \\ C_0 & (r \gg R_{COR}), \end{cases} \tag{2}$$

where $d = 2$ is the Euclidean dimension of the space in which aggregation occurs, D_f is the fractal dimension of the aggregate, and R_{COR} is the correlation length (Meakin, 1984a). If M is the mass contained in a circle of radius r, then D_f is defined by $M \sim r^{D_f}$. For an ordinary two-dimensional object, $D_f = 2$. Lower values correspond to tenuous, stringy structures. The fractal dimensions and correlation lengths are obtained by a least-squares fit of a straight line to the initial part of the curves in Fig. 3. The intersection of this line with the horizontal line $C(r) = C_0$ gives R_{COR}, as shown. The correlation length varies with concentration according to $C_0 \sim R_{COR}^{D_f-d}$ (Meakin, 1984a; Martin and Wilcoxon, 1989). If $D_f = 1.5$, then $R_{COR} \sim 1/C_0^2$, and if $D_f = 1.75$, then $R_{COR} \sim 1/C_0^4$. So, as $C_0 \to 0$, $R_{COR} \to \infty$, as seen in Fig. 3 b (though in Fig. 3 b both R_{COR} and D_f vary with C_0).

In Fig. 3 a, the structure at $t = 0$ is not fractal but uniform, and $C(0) = 1$, $C(r) = C_0$ for all $r > 0$. As

a. C = 0.10
P_{AGG} = 1
t = 0

b. C = 0.10
P_{AGG} = 1
t = 10

c. C = 0.10
P_{AGG} = 1
t = 100

d. C = 0.10
P_{AGG} = 1
t = 1000

e. C = 0.10
P_{AGG} = 1
$t \rightarrow \infty$

f. C = 0.05
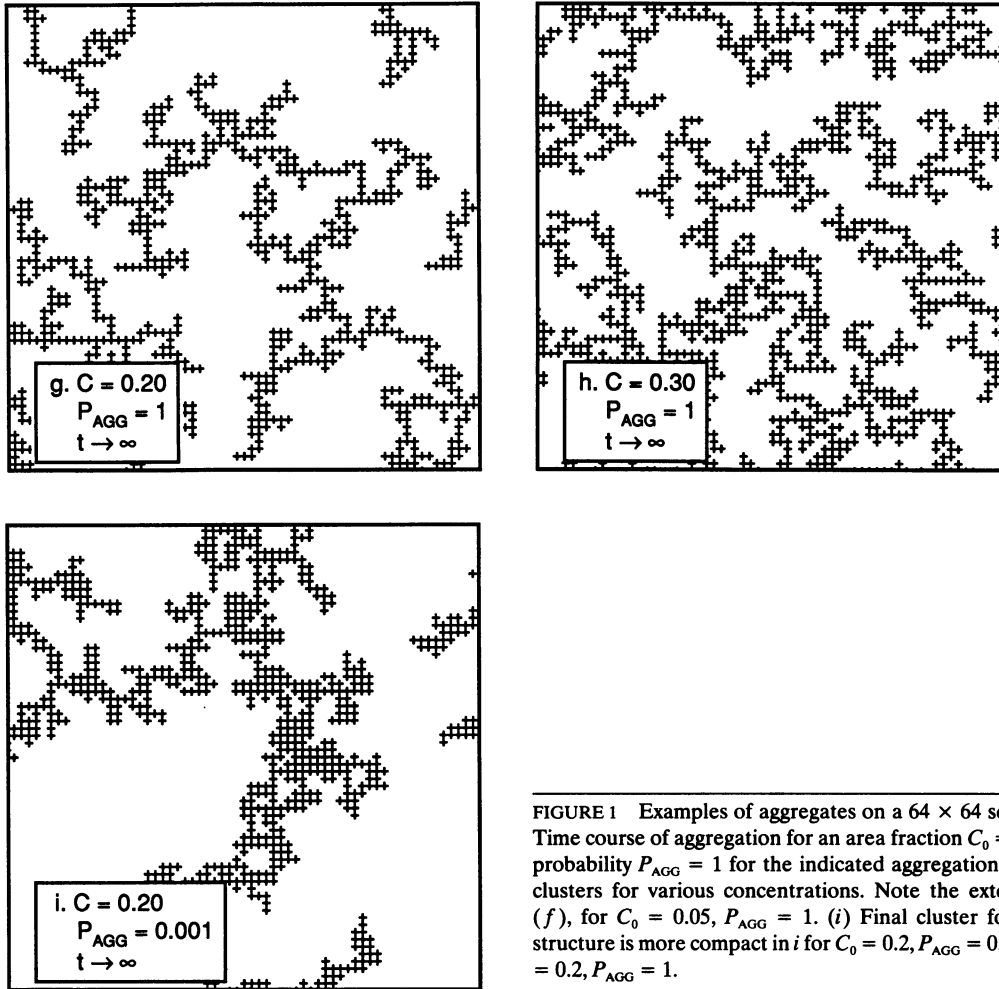P_{AGG} = 1
$t \rightarrow \infty$

FIGURE 1   Examples of aggregates on a 64 × 64 square lattice. (a–e) Time course of aggregation for an area fraction $C_0 = 0.1$ and a sticking probability $P_{AGG} = 1$ for the indicated aggregation times. (f–h) Final clusters for various concentrations. Note the extended structure in (f), for $C_0 = 0.05$, $P_{AGG} = 1$. (i) Final cluster for small P_{AGG}. The structure is more compact in i for $C_0 = 0.2, P_{AGG} = 0.001$ than in g for $C_0 = 0.2, P_{AGG} = 1$.

aggregation continues, fractal structure builds up, and by $t = 10^4$, there is fractal structure extending over a range $r = 1$ to 10. The variation in $C(r)$ with C_0 and P_{AGG} is shown in Fig. 3, b and c; these results are discussed later.

Time autocorrelation functions have been studied extensively as probes of aggregation (Meyer and Schindler, 1988; Elson and Qian, 1989; Palmer and Thompson, 1989). The simplest of these is the first-order time autocorrelation function

$$G(\tau) = \langle \delta F(\tau) \delta F(0) \rangle / \langle F^2 \rangle, \tag{3}$$

where F is the fluorescence intensity and δF is the fluctuation in F. For a single-component system, $G(0)$ gives the number of independently moving particles. It may be possible to obtain the number of monomers and oligomers in an aggregating system by measurement of higher autocorrelation functions, but in practice this is complex (Palmer and Thompson, 1989). A spatial correlation function can be obtained by scanning fluorescence correlation spectroscopy (Petersen, 1986).

The effect of aggregates on the diffusion of inert tracers

An aggregate (either a cluster of membrane proteins or a cluster of gel-phase lipid) may act as an obstacle to lateral diffusion. This effect can be evaluated from the model. The aggregation process is stopped, an inert point tracer is introduced, and the tracer executes a random walk. Motion of the tracer is obstructed by the aggregate, but the tracer does not adhere to the aggregate. The mean-square displacement of the tracer is calculated as a function of time, yielding the concentration-dependent, distance-dependent diffusion coefficient $D^*(C, r)$.

Here the usual diffusion coefficient is generalized to include the effect of the distance over which diffusion is measured (Saxton, 1989). The basic physical idea is that a label is produced at $t = 0$, and its diffusion is then measured over a distance r. In measurements by fluorescence photobleaching recovery, r is of the order of the radius of the photobleached area, typically ~ 1 μm, but
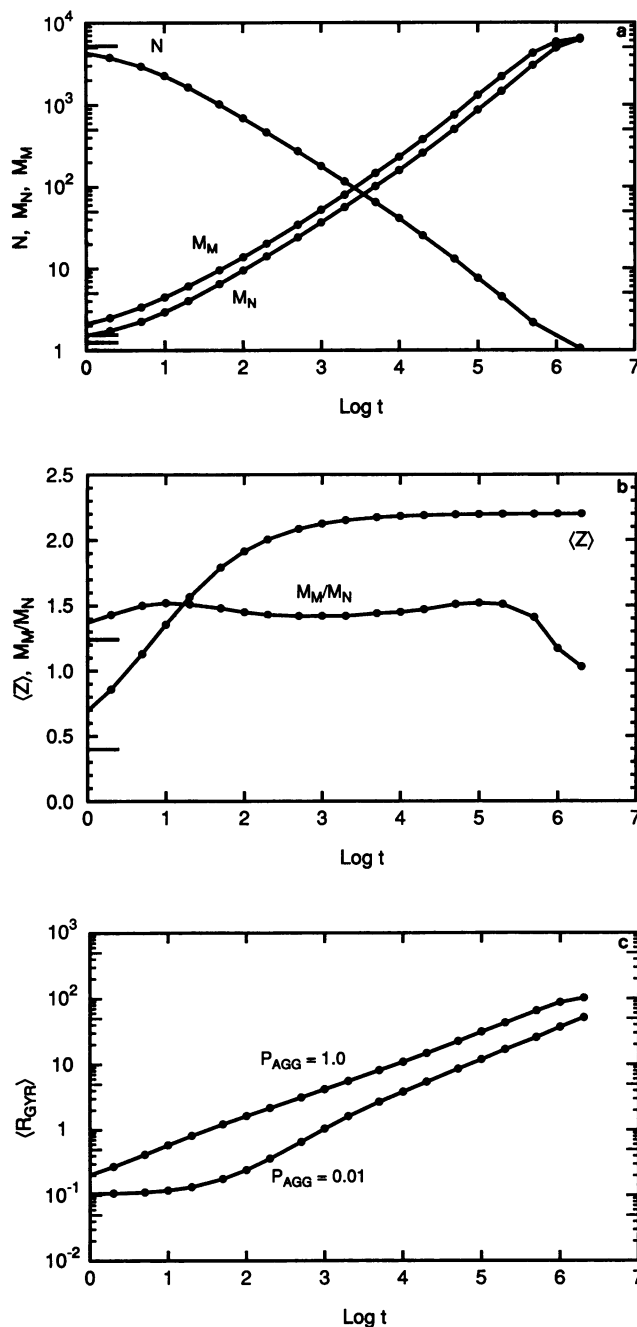
FIGURE 2 Cluster properties as a function of aggregation time for $C_0 = 0.1$, $P_{AGG} = 1$. Horizontal lines on the left axis indicate the initial values. To evaluate statistical error, two independent runs for $P_{AGG} = 1$, $C_0 = 0.1$ were compared. The curves were practically indistinguishable. (*a*) Number of clusters N, number-average cluster mass M_N, and mass-average cluster mass M_M. (*b*) Average coordination number $\langle Z \rangle$ and ratio M_M/M_N. (*c*) Number-average radius of gyration for $P_{AGG} = 1$ and $P_{AGG} = 0.01$.
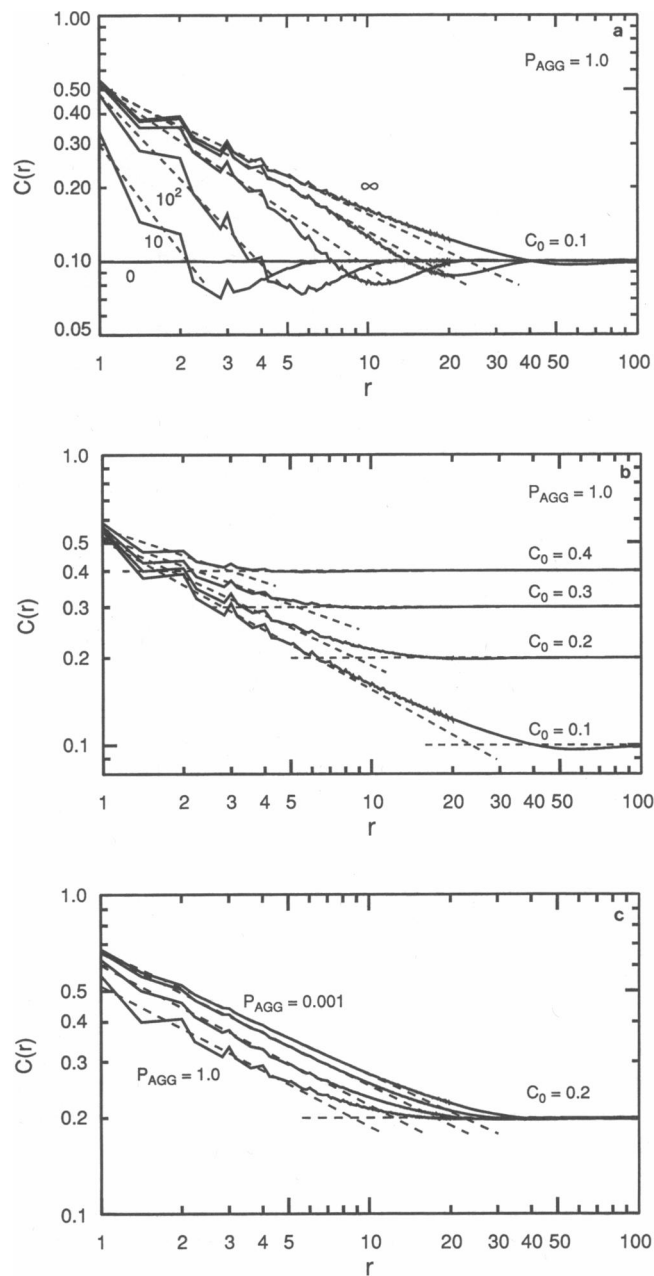
FIGURE 3 Log–log plot of the particle–particle correlation function $C(r)$ as a function of r. Three independent runs for $C_0 = 0.2$, $P_{AGG} = 1$, $t \rightarrow \infty$ gave indistinguishable curves. (*Dashed lines*) Linear fit to the initial points of the curve. The intersection of these lines with the line $C(r) = C_0$ yields the correlation length R_{COR}. The peaks in $C(r)$ for small r reflect lattice structure. (*a*) $C(r)$ during the aggregation process for $C_0 = 0.1$, $P_{AGG} = 1.0$, for aggregation times of 0, 10, 10^2, 10^3, 10^4, and ∞. (*b*) $C(r)$ for the final clusters for $P_{AGG} = 1.0$, $C_0 = 0.1$, 0.2, 0.3, and 0.4. As the concentration decreases, the correlation length increases. (*c*) $C(r)$ for the final clusters for $C_0 = 0.2$, $P_{AGG} = 0.001$, 0.01, 0.1, and 1.0. As P_{AGG} decreases, the correlation length increases.

in measurements by excimer formation or fluorescence quenching, $r \sim$ 1–10 nm, the average initial separation of the interacting species (Eisinger et al., 1986).

Fig. 4 shows the diffusion coefficient in the presence of square obstacles, random point obstacles, and aggregates. The area fraction of obstacles is constant, $C_0 = 0.3$, but the effects of the obstacles on diffusion are much different. Compact obstacles are much less effective barriers to diffusion of a tracer than the same area fraction of random point obstacles is (Eisinger et al., 1986). Cluster–cluster aggregates, however, are much more effective barriers than the same area fraction of random points. Thus, if a fixed number of isolated monomers collects to form cluster–cluster aggregates, their effect on lateral diffusion of an inert tracer will increase, but if the same monomers collect into compact structures, their effect will decrease.

The distance-dependent diffusion coefficient shows that for compact obstacles the effect of obstacle size is similar for short-range and long-range diffusion measurements, but the effect of aggregation is clear only in long-range measurements.

One way of visualizing the effectiveness of a type of obstacle is by finding the concentration of random points giving the same long-range diffusion coefficient. Fig. 5 shows the concentration dependence of the long-range diffusion coefficient $D^*(C, \infty)$ for an inert tracer obstructed by random points, random nonoverlapping squares of sides 1, 2, and 4, and the final clusters for $P_{AGG} = 0.01$ and $P_{AGG} = 1$. Cluster–cluster aggregates are remarkably effective barriers to long-range lateral diffusion. An area fraction of obstacles as low as 0.05 can

FIGURE 5 Concentration dependence of the long-range diffusion coefficient $D^*(C, \infty)$ of an inert tracer for the indicated types of obstacles: nonoverlapping random squares of sides 1, 2, and 4; random points; and final cluster–cluster aggregates for $P_{AGG} = 0.01$ and $P_{AGG} = 1$. The percolation threshold $P_C = 0.407$ is indicated. As the concentration of random point obstacles is increased to this value, the percolating cluster of unblocked sites disappears and the diffusion coefficient goes to zero (in an infinite system).

lower D^* to 38% of its value in an unobstructed bilayer. A final cluster at a concentration $C_0 = 0.2$, $P_{AGG} = 1$ is as effective an obstacle as random points at $C_0 \simeq 0.37$.

Why are the aggregates such effective obstacles, especially at low concentrations? First, the aggregates contain many dead ends in which an inert tracer could be trapped temporarily, as shown in Fig. 1. Second, the aggregates are extended structures, and become more extended as the density of aggregating particles decreases. This is shown qualitatively in Fig. 1, in the examples of final clusters for various concentrations, and quantitatively in Fig. 3 b, a log–log plot of the particle–particle correlation function for various concentrations. As the density decreases, the correlation length increases, and the fractal dimension decreases. Why do the clusters become more extended? The clusters are fractal, and cannot penetrate each other very much, so the fractal dimension of the aggregate is low. As the concentration decreases, the clusters penetrate each other less, and the fractal dimension decreases (Martin and Hurd, 1987; Kolb et al., 1985; Vicsek, 1989). In contrast, in the diffusion-limited aggregation model, single particles diffuse and penetrate the growing cluster. Penetration is easier, and the fractal dimension is higher (Meakin, 1988; Vicsek, 1989).

These results are for particles which adhere on contact with probability 1. A lower probability leads to structures that are more compact (Fig. 1 i) and less effective obstacles (Fig. 5). At any fixed concentration of obstacles, the diffusion coefficient of inert tracers increases as P_{AGG} decreases. This effect can be significant
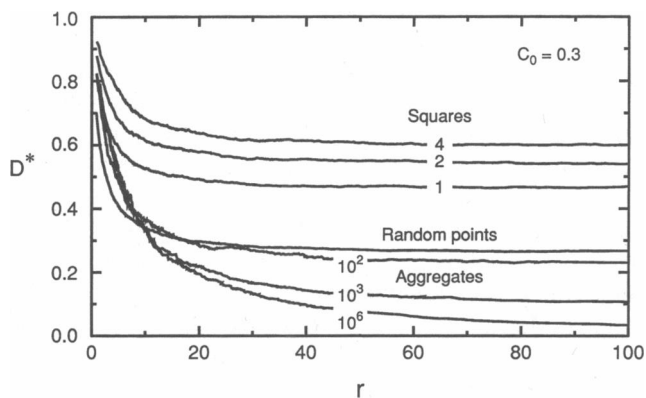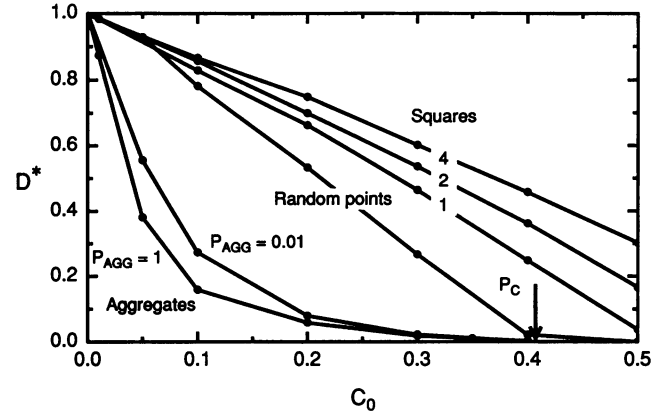
FIGURE 4 Distance-dependent lateral diffusion coefficient $D^*(r)$ of an inert tracer as a function of the distance over which diffusion is measured. Results are shown for an area fraction $C_0 = 0.3$ for the indicated obstacles: nonoverlapping random squares of sides 1, 2, and 4; random points; and cluster–cluster aggregates ($P_{AGG} = 1$) for the indicated aggregation times. The curves show the magnitude of statistical noise in the results.

(for example, at $C_0 = 0.1$, as P_{AGG} decreases from 1 to 0.01, D^* increases by a factor of 1.7), but the values of D^* are still much lower than for random point obstacles.

Table 1 shows the variation in fractal dimension D_f, correlation length R_{COR}, and average coordination number $\langle Z \rangle$ with sticking probability P_{AGG} and concentration C_0 for final clusters. At constant P_{AGG}, as the concentration increases, the structure becomes more compact, as shown by the increase in fractal dimension, the decrease in correlation length, and the increase in $\langle Z \rangle$. At constant concentration, as P_{AGG} decreases, the fractal dimension increases, indicating a more compact structure, but the correlations extend over longer distances. Some literature values of D_f are also given (Kolb and Herrmann, 1985; Vicsek, 1989). Flocculation corresponds to the low-density limit of the CCA model, gelation, to the high-density limit. The values obtained here fall between these limits. The fractal dimension of diffusion-limited aggregates (DLA) is higher than that of most of the cluster–cluster aggregates, as already mentioned. The fractal dimension for a percolating cluster of random points at the percolation threshold is higher than that of any of the aggregates. The aggregates are stringier than percolation clusters, and better obstacles.

Annealing leads to more compact structures. In the calculations presented here, initial binding occurs with a probability P_{AGG} that may be less than one, but once binding occurs it is irreversible. Shih et al. (1987) presented a CCA model in which bonds can be broken at a rate proportional to $\exp(-nE/T)$, where n is the number of nearest neighbors, E is the binding energy, and T is the temperature. In this model, a ramified cluster can become compact. Such a temperature-dependent model interpolates between the compact and extended structures presented here.

Lateral diffusion of a fluorescent lipid was measured by fluorescence photobleaching recovery during lateral

TABLE 1 Properties of final clusters

P_{AGG}	C_0	D_f	R_{COR}	$\langle Z \rangle$
1.0	0.050	1.46	72.56	2.190
1.0	0.100	1.50	24.62	2.202
1.0	0.200	1.56	8.66	2.232
1.0	0.300	1.67	5.29	2.278
1.0	0.400	1.69	3.00	2.342
1.0	0.200	1.56	8.66	
0.1	0.200	1.56	12.27	
0.01	0.200	1.58	17.51	
0.001	0.200	1.61	22.23	
Flocculation		1.42 ± 0.05		
Gelation		1.75 ± 0.07		
DLA		1.70 ± 0.06		
Percolation		1.90		

phase separation in various mixtures of phosphatidylcholines (Vaz et al., 1989, 1990; Bultmann et al., 1991). In a mixture of dimyristoylphosphatidylcholine and distearoylphosphatidylcholine, a small fraction of gel-phase lipid, ~20%, was sufficient to block long-range diffusion, implying the existence of a reticular structure of gel-phase lipid. Fig. 5 shows that, for an area fraction of 0.2, long-range diffusion is still allowed in the presence of an aggregate, though at a significantly reduced rate. Cluster–cluster aggregates of particles with hard-disk interactions are very effective obstacles to diffusion, but even they are not effective enough to account for the results observed (Vaz et al., 1989, 1990; Bultmann et al., 1991). Anisotropic growth may explain their results, particularly if the cause of the anisotropy is the dipole–dipole interaction, which is long-range (Saxton, 1991).

Lateral and rotational diffusion of clusters

To characterize an aggregation process, one could measure lateral and rotational diffusion of the aggregating species, and lateral diffusion of an inert species. In the model, the lateral diffusion coefficient of a cluster is assumed to be inversely proportional to mass, so it is easy to evaluate the average $D_T^*(CL)$ during the aggregation process. The rotational diffusion coefficient of a cluster is inversely proportional to the square of the hydrodynamic radius of the cluster (Saffman and Delbrück, 1975), and falls off rapidly with cluster size: $D_R^*(CL) = 1$ for single points, 0.1667 for pairs, 0.0732 for bent triples, and 0.0526 for linear triples (Eq. 1).

Fig. 6 shows the change in diffusion coefficients during the aggregation process for $C_0 = 0.1$. The rapid decrease in the translational diffusion coefficient of the aggregating species is a result of the assumption that $D_T(CL)$ is inversely proportional to mass; if $D_T(CL)$ follows the Saffman-Delbrück equation, the decrease is much slower. As expected (Cherry and Godfrey, 1981), rotational diffusion of the aggregating species is extremely sensitive to the initial stages of aggregation. Long-range lateral diffusion of an inert tracer (as measured by fluorescence photobleaching recovery) is insensitive to the initial stages of aggregation but is an effective probe of the final stages. Measurements of rotational diffusion of the aggregating species and lateral diffusion of an inert species are thus complementary.

Two average rotational diffusion coefficients are shown: the number average $D_R^*(N)$, which is appropriate if each cluster has one and only one label, and the mass average $D_R^*(M)$, which is appropriate if each monomer is labeled, and aggregation does not affect the quantum yield of the labels.

This calculation is a zeroth-order approximation. The aggregation calculations ought to be carried out using
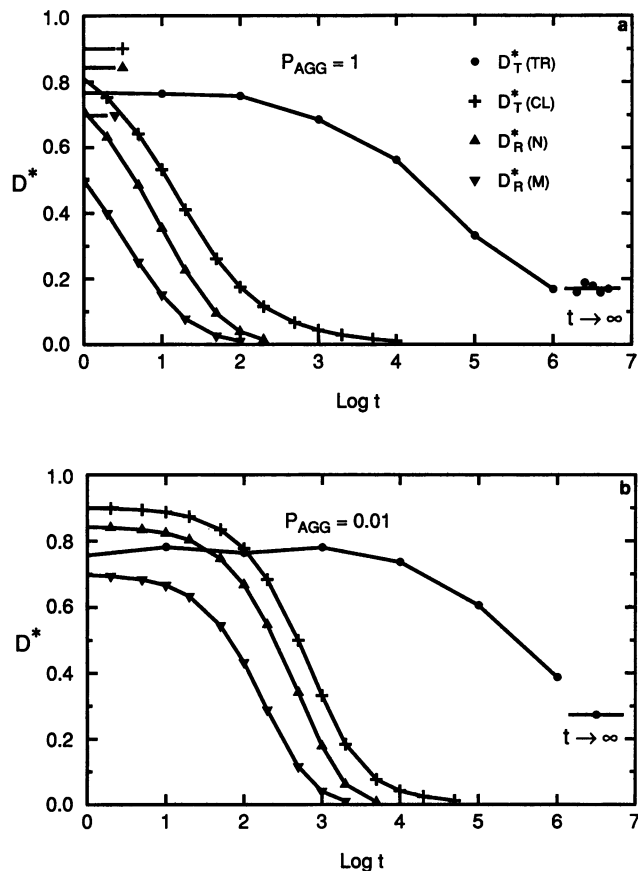
FIGURE 6 Diffusion coefficients as a function of aggregation time for $C_0 = 0.1$, and (a) $P_{AGG} = 1$, (b) $P_{AGG} = 0.01$. Long-range translational diffusion coefficient $D_T^*(TR)$ of an inert tracer; average translational diffusion coefficient $D_T^*(CL)$ of a cluster; number-average rotational diffusion coefficient $D_R^*(N)$ of a cluster; mass-average rotational diffusion coefficient $D_R^*(M)$. In a, the horizontal lines at the left axis show initial values. The diffusion coefficient of the inert tracer is normalized to one for zero concentration of obstacles; the diffusion coefficients of the clusters are normalized to one for monomers. In a, values from five independent calculations for $t \to \infty$ are shown; in b, one value.

the Saffman-Delbrück equation or its generalization (Hughes et al., 1982) for the translational diffusion coefficient, instead of a diffusion coefficient inversely proportional to mass. The results of Wiegel (1979) for the lateral and rotational diffusion coefficients of a porous aggregate could also be used.

REFERENCES

Bultmann, T., W. L. C. Vaz, E. C. C. Melo, R. B. Sisk, and T. E. Thompson. 1991. Fluid-phase connectivity and translational diffusion in a eutectic, two-component, two-phase phosphatidylcholine bilayer. Biochemistry. 30:5573–5579.

Cherry, R. J., and R. E. Godfrey. 1981. Anisotropic rotation of bacteriorhodopsin in lipid membranes: comparison of theory with experiment. Biophys. J. 36:257–276.

Clegg, R. M., and W. L. C. Vaz. 1985. Translational diffusion of proteins and lipids in artificial lipid bilayer membranes. A comparison of experiment with theory. In Progress in Protein-Lipid Interactions, Vol. 1. A. Watts and J. J. H. H. M. De Pont, editors. Elsevier, Amsterdam. 173–229.

Eisinger, J., J. Flores, and W. P. Petersen. 1986. A milling crowd model for local and long-range obstructed lateral diffusion. Biophys. J. 49:987–1001.

Elson, E. L., and H. Qian. 1989. Interpretation of fluorescence correlation spectroscopy and photobleaching recovery in terms of molecular interactions. Methods Cell Biol. 30:307–332.

Flörsheimer, M., and H. Möhwald. 1989. Development of equilibrium domain shapes in phospholipid monolayers. Chem. Phys. Lipids 49:231–241.

Hoshen, J., and R. Kopelman. 1976. Percolation and cluster distribution. I. Cluster multiple labeling technique and critical concentration algorithm. Phys. Rev. B14:3438–3445.

Hughes, B. D., B. A. Pailthorpe, L. R. White, and W. H. Sawyer. 1982. Extraction of membrane microviscosity from translational and rotational diffusion coefficients. Biophys. J. 37:673–676.

Jullien, R., and R. Botet. 1987. Aggregation and Fractal Aggregates. World Scientific, Singapore. 120 pp.

Kolb, M. 1984. Unified description of static and dynamic scaling for kinetic cluster formation. Phys. Rev. Lett. 53:1653–1656.

Kolb, M., and H. J. Herrmann. 1985. The sol-gel transition modelled by irreversible aggregation of clusters. J. Phys. A18:L435–L441.

Kolb, M., and R. Jullien. 1984. Chemically limited versus diffusion limited aggregation. J. Physique Lett. 45:L977–L981.

Kolb, M., R. Botet, and R. Jullien. 1983. Scaling of kinetically growing clusters. Phys. Rev. Lett. 51:1123–1126.

Kolb, M., R. Jullien, and R. Botet. 1985. Scaling properties of cluster and particle aggregation. In Scaling Phenomena in Disordered Systems. R. Pynn and A. Skjeltorp, editors. Plenum Press, New York. 71–78.

Martin, J. E., and A. J. Hurd. 1987. Scattering from fractals. J. Appl. Cryst. 20:61–78.

Martin, J. E., and J. P. Wilcoxon. 1989. Spatial correlations and growth in dilute gels. Phys. Rev. A39:252–258.

Meakin, P. 1983. Formation of fractal clusters and networks by irreversible diffusion-limited aggregation. Phys. Rev. Lett. 51:1119–1122.

Meakin, P. 1984a. Diffusion-controlled aggregation on two-dimensional square lattices: results from a new cluster-cluster aggregation model. Phys. Rev. B29:2930–2942.

Meakin, P. 1984b. The effects of rotational diffusion on the fractal dimensionality of structures formed by cluster-cluster aggregation. J. Chem. Phys. 81:4637–4639.

Meakin, P. 1984c. Diffusion-limited aggregation in three dimensions: results from a new cluster-cluster aggregation model. J. Coll. Interface Sci. 102:491–504.

Meakin, P. 1985. Off lattice simulations of cluster-cluster aggregation in dimensions 2-6. *Phys. Lett.* 107A:269–272.

Meakin, P. 1988. The growth of fractal aggregates and their fractal measures. *In* Phase Transitions and Critical Phenomena, Vol. 12. C. Domb and J. L. Lebowitz, editors. Academic Press, London. 335–489.

Meakin, P., T. Vicsek, and F. Family. 1985. Dynamic cluster-size distribution in cluster-cluster aggregation: effects of cluster diffusivity. *Phys. Rev.* B31:564–569.

Meyer, T., and H. Schindler. 1988. Particle counting by fluorescence correlation spectroscopy: simultaneous measurement of aggregation and diffusion of molecules in solutions and in membranes. *Biophys. J.* 54:983–993.

Palmer III, A. G., and N. L. Thompson. 1989. Fluorescence correlation spectroscopy for detecting submicroscopic clusters of fluorescent molecules in membranes. *Chem. Phys. Lipids.* 50:253–270.

Petersen, N. O. 1986. Scanning fluorescence correlation spectroscopy. I. Theory and simulation of aggregation measurements. *Biophys. J.* 49:809–815.

Petersen, N. O., D. C. Johnson, and M. J. Schlesinger. 1986. Scanning fluorescence correlation spectroscopy. II. Application to virus glycoprotein aggregation. *Biophys. J.* 49:817–820.

Press, W. H., B. P. Flannery, S. A. Teukolsky, and W. T. Vetterling. 1986. Numerical Recipes. The Art of Scientific Computing. Cambridge University Press, Cambridge. 449–453.

Saffman, P. G., and M. Delbrück. 1975. Brownian motion in biological membranes. *Proc. Natl. Acad. Sci. USA.* 72:3111–3113.

Saxton, M. J. 1987. Lateral diffusion in an archipelago: the effect of mobile obstacles. *Biophys. J.* 52:989–997.

Saxton, M. J. 1989. Lateral diffusion in an archipelago: distance dependence of the diffusion coefficient. *Biophys. J.* 56:615–622.

Saxton, M. J. 1991. Lateral diffusion in an archipelago: shifts in the percolation threshold. *Biophys. J.* 59:627a. (Abstr.)

Schlüter, K., and D. Drenckhahn. 1986. Co-clustering of denatured hemoglobin with band 3: its role in binding of autoantibodies against

band 3 to abnormal and aged erythrocytes. *Proc. Natl. Acad. Sci. USA.* 83:6137–6141.

Shih, W. Y., I. A. Aksay, and R. Kikuchi. 1987. Reversible-growth model: cluster-cluster aggregation with finite binding energies. *Phys. Rev.* A36:5015–5019.

Sun, J., and M. Petersheim. 1990. Lanthanide(III)-phosphatidic acid complexes: binding site heterogeneity and phase separation. *Biochim. Biophys. Acta.* 1024:159–166.

Synge, J. L., and B. A. Griffith. 1949. Principles of Mechanics. 2nd edition. McGraw-Hill, New York. 189–193.

Tanford, C. 1961. Physical Chemistry of Macromolecules. John Wiley and Sons, New York. 146–147.

Vaz, W. L. C., E. C. C. Melo, and T. E. Thompson. 1989. Translational diffusion and fluid domain connectivity in a two-component, two-phase phospholipid bilayer. *Biophys. J.* 56:869–876.

Vaz, W. L. C., E. C. C. Melo, and T. E. Thompson. 1990. Fluid phase connectivity in an isomorphous, two-component, two-phase phosphatidylcholine bilayer. *Biophys. J.* 58:273–275.

Velez, M., K. F. Barald, and D. Axelrod. 1990. Rotational diffusion of acetylcholine receptors on cultured rat myotubes. *J. Cell Biol.* 110:2049–2059.

Vicsek, T. 1989. Fractal Growth Phenomena. World Scientific, Singapore. 355 pp.

Vicsek, T., and F. Family. 1984. Critical dynamics in cluster-cluster aggregation. *In* Kinetics of Aggregation and Gelation. F. Family and D. P. Landau, editors. Elsevier, Amsterdam. 111–115.

Waugh, S. M., B. M. Willardson, R. Kannan, R. J. Labotka, and P. S. Low. 1986. Heinz bodies induce clustering of band 3, glycophorin, and ankyrin in sickle cell erythrocytes. *J. Clin. Invest.* 78:1155–1160.

Weinstein, R. S., J. K. Khodadad, and T. L. Steck. 1979. The band 3 protein intramembrane particle of the human red blood cell. *In* Membrane Transport in Erythrocytes. U. V. Lassen, H. H. Ussing, and J. O. Wieth, editors. Munksgaard, Copenhagen. 35–50.

Wiegel, F. W. 1979. Translational friction coefficient of a permeable cylinder in a sheet of viscous fluid. *J. Phys.* A12:2385–2392.